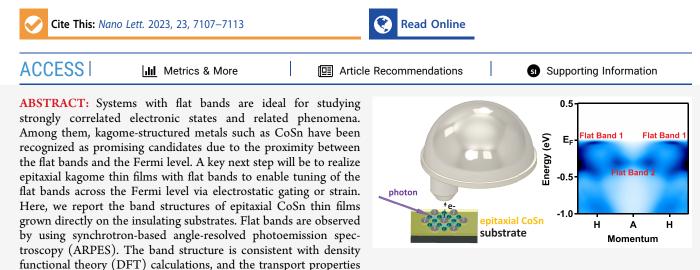Letter

Epitaxial Kagome Thin Films as a Platform for Topological Flat Bands

Shuyu Cheng, M. Nrisimhamurty, Tong Zhou, Núria Bagués, Wenyi Zhou, Alexander J. Bishop, Igor Lyalin, Chris Jozwiak, Aaron Bostwick, Eli Rotenberg, David W. McComb,* Igor Žutić,* and Roland K. Kawakami*

Read Online

ACCESS | Metrics & More | Article Recommendations | SI Supporting Information

ABSTRACT: Systems with flat bands are ideal for studying strongly correlated electronic states and related phenomena. Among them, kagome-structured metals such as CoSn have been recognized as promising candidates due to the proximity between the flat bands and the Fermi level. A key next step will be to realize epitaxial kagome thin films with flat bands to enable tuning of the flat bands across the Fermi level via electrostatic gating or strain. Here, we report the band structures of epitaxial CoSn thin films grown directly on the insulating substrates. Flat bands are observed by using synchrotron-based angle-resolved photoemission spectroscopy (ARPES). The band structure is consistent with density functional theory (DFT) calculations, and the transport properties are quantitatively explained by the band structure and semiclassical transport theory. Our work paves the way to realize flat band-induced phenomena through fine-tuning of flat bands in kagome materials.

KEYWORDS: kagome material, angle-resolved photoemission spectroscopy, flat band, molecular beam epitaxy

Strongly correlated electronic systems are one of the focus of condensed matter physics due to the emergence of interesting many-body ground states. Materials with dispersionless bands, i.e., flat bands, are ideal systems for studying the physics of strongly correlated electronic states due to the smaller bandwidth W as compared to the Coulomb repulsion U. One noted example is the flat band in twisted bilayer graphene, which is responsible for various correlated phenomena such as tunable superconductivity,[1,2] magnetism,[3] and metal-to-insulator transitions.[4] Another important class of materials exhibiting flat bands is those composed of quasi-two-dimensional (2D) kagome lattices. Examples in this family include CoSn,[5,6] Fe_3Sn_2,[7] $Co_3Sn_2S_2$,[8] YMn_6Sn_6,[9] and Ni_3In.[10] In 2D kagome lattices, the flat band emerges due to the destructive phase interference of the electronic wave functions within the hexagons of the kagome lattice. This mechanism generates electronic states confined within these hexagons in real space and appears as nondispersing bands in momentum space.[5,6,11] Theoretically, a 2D kagome lattice generates a perfect flat band in the tight-binding model considering only nearest-neighbor hopping. In real materials, the actual band structure can deviate from the ideal case due to the existence of additional hopping terms and spin−orbit coupling.[5]

For realizing flat-band-induced phenomena in kagome metals, it is important to fine-tune the flat band position relative to the Fermi level, since many physical properties are dominated by states at the Fermi level. To this end, synthesizing epitaxial thin films of kagome metals provides several strategies for tuning the flat bands. The highly controlled growth process using molecular beam epitaxy (MBE) allows one to chemically dope the material, while after the growth, device patterning and voltage gating are another way to tune the flat bands. In addition, anisotropic strains can be applied to thin films through either epitaxial growth or mechanical methods. All of these potential advantages provide strong motivation for investigating flat-band-hosting kagome thin films. While tunneling spectroscopy has provided indirect evidence for the existence of flat bands in epitaxial FeSn films,[12] direct observation of flat bands in kagome thin films has been missing.

In terms of material selection, CoSn stands out due to the existence of flat bands several hundreds of meV below the Fermi level and spreads across a large portion of the Brillouin zone (BZ).[13] In CoSn bulk crystals, such flat bands have been
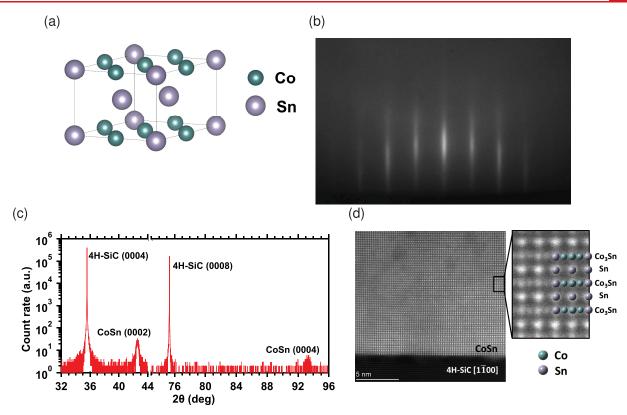
Figure 1. Sample growth and characterization. (a) Crystal structure of CoSn. (b) RHEED pattern of a 35 nm CoSn(0001) thin film grown on 4H-SiC(0001) substrates. (c) X-ray diffraction of a 35 nm CoSn(0001) thin film. (d) Atomic-resolution HAADF-STEM image of a CoSn(0001) thin film grown on the 4H-SiC(0001) substrate viewed along the 4H-SiC[$1\bar{1}00$] direction.

confirmed by angle-resolved photoemission spectroscopy (ARPES) experiments.[5,6,14] Recent work further established the connection between flat bands in CoSn and the observed large resistance within the kagome plane as compared to perpendicular to the kagome plane.[14] Regarding the thin film growth, there has been one work reporting epitaxial CoSn thin films on metallic buffer layers by magnetron sputtering.[15] Although the previously reported sputtered CoSn thin films showed physical properties that are consistent with the bulk crystals, the direct evidence of flat bands in CoSn thin films remains elusive.[15] Furthermore, a challenge for epitaxial kagome films is the difficulty of growing continuous films directly onto insulating substrates,[16] which are favored for voltage gating and transport studies.

In this paper, we demonstrate epitaxial CoSn thin films grown on insulating substrates as a promising platform to realize flat-band physics. The growth of (0001)-oriented CoSn thin films on insulating MgO(111) and 4H-SiC(0001) substrates was enabled by a three-step MBE growth recipe. Using synchrotron-based ARPES, we directly measured the band structure of the CoSn thin films and revealed multiple flat bands. At the Γ point, spin−orbit coupling (SOC) gaps were observed between one of the flat bands and the quadratic bands, suggesting the nontrivial topology of this flat band. Using density functional theory (DFT) calculations, we studied the tunability of the flat bands through carrier doping and found that the calculations are consistent with the ARPES experiments. Finally, we measured the transport properties of CoSn and quantitatively explained the results using band structure and semiclassical transport theory.

The CoSn thin films were grown on MgO(111) or 4H-SiC(0001) substrates by MBE by using a three-step recipe.

First, a 5 nm seed layer was deposited at 500 °C (470 °C) on 4H-SiC(0001) (MgO(111)) substrates, followed by a 15−20 nm continuation layer grown at 100 °C. The third step is the growth of a terminating layer of 5−10 nm CoSn at 300 °C. Details of the growth (and other methods) are provided in the Supporting Information (SI) section S1.

Figure 1b shows the *in situ* reflection high-energy electron diffraction (RHEED) pattern of a 35 nm CoSn thin film grown on a 4H-SiC(0001) substrate. The streaky RHEED pattern indicates epitaxial growth and two-dimensional surfaces with a finite terrace width. The X-ray diffraction (XRD) data of a 35 nm CoSn thin film grown on a 4H-SiC(0001) substrate is shown in Figure 1c (the RHEED and XRD data of CoSn films grown on MgO(111) substrates are provided in the SI section S2). Besides the substrate peaks at 32.57° and 75.34°, two additional peaks show up at 42.57° and 93.34°, corresponding to CoSn (0002) and (0004) peaks, respectively. The out-of-plane lattice constant extracted from the XRD scan is 4.254 Å, which is in good agreement with the previous studies on bulk crystals[17] and sputtered thin films.[15]

High-angle annular dark-field (HAADF) scanning transmission electron microscopy (STEM) imaging was performed to examine the crystalline characteristics of the CoSn thin film (see SI section S1.2 for methods). Figure 1d shows an atomic-resolution HAADF-STEM image of a 35 nm CoSn(0001) thin film on 4H-SiC(0001) viewed along the 4H-SiC[$1\bar{1}00$] axis. The HAADF-STEM image reveals the alternating stacking sequence of one Co_3Sn kagome layer and one Sn_2 honeycomb layer, which is expected for CoSn (Figure 1a). The brightness of atomic columns in the HAADF-STEM image is approximately proportional to the square of the atomic number (Z); consequently, Sn (Z = 50) atom columns appear
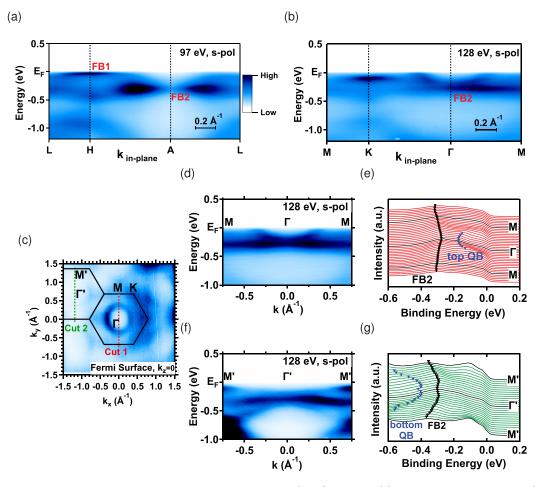
Figure 2. Observation of flat bands in a 25 nm CoSn thin film on the 4H-SiC(0001) substrate. (a) ARPES spectra in the $k_z = \pi$ (mod 2π) plane, measured with 97 eV s-polarized photons. (b) ARPES spectra in the $k_z = 0$ (mod 2π) plane, measured with 128 eV s-polarized photons. (c) Fermi surface of the $k_z = 0$ (mod 2π) plane. The black hexagons represent BZs. (d) ARPES spectra along the M-Γ-M direction ("Cut 1" in (c)) in the first BZ. (e) EDCs of (d). The black and blue delta symbols mark the position of peaks from FB2 and the top QB, respectively. (f) ARPES spectrum along the M′-Γ′-M′ direction ("Cut 2" in (c)) in the second BZ. (g) EDCs of (f). The black and blue delta symbols mark the position of peaks from FB2 and the bottom QB, respectively.

as brighter columns, while the mixture of CoSn atom columns and Co ($Z = 27$) atom columns appear dimmer. Although the sequence of the alternating stacking of one Co_3Sn layer and one Sn_2 layer is predominant across the film, in some regions closer to the interface, the sequence is alerted by the addition of extra Co_3Sn layers (SI section S3).

Having synthesized the epitaxial CoSn thin films, the questions one would raise are whether or not our thin films have flat bands and whether or not the flat bands are topologically nontrivial if they exist. The most straightforward method to answer these questions is to directly measure the band structures using ARPES. In this study, we utilized the synchrotron-based ARPES to map the band structures of 25 nm CoSn thin films grown on MgO(111) and 4H-SiC(0001) substrates (see SI section S1.3 for methods). In the following discussion, we will mainly focus on the band structures of CoSn on 4H-SiC(0001) substrates, while the band structures of CoSn on the MgO(111) substrate are presented in SI section S4.1. Figure 2a shows the band structures measured using s-polarized (s-pol) photons with 97 eV energy, which corresponds to the $k_z = \pi$ (mod 2π) plane in the momentum space (see SI section S4.2 for k_z dependence of the ARPES spectrum and SI section S4.3 for ARPES spectra taken with p-polarized light). In this plane, two dispersionless bands can be

observed: one band centers around the H point (labeled as "FB1" in Figure 2a) close to the Fermi level, while the other band ("FB2") resides deeper below the Fermi level and spreads over almost the entire BZ. Lorentzian fitting of energy distribution curves (EDCs) around the H point gives a binding energy of −0.04 eV for FB1, with effective mass $m^* = 16.7\ m_0$ along the H-L direction, where m_0 is the mass of free electrons. Meanwhile, fitting EDCs at the A and L points yields −0.31 and −0.32 eV binding energies, respectively (see SI section S4.4 for details).

It is noteworthy that FB1 is reported to be accountable for the anomalous anisotropic transport properties and orbital magnetic moment in bulk CoSn, due to its proximity to the Fermi level.[14] Another work demonstrates that tuning FB1 to the Fermi level through chemical doping induces antiferromagnetic ordering at low temperatures.[18] In our work, FB1 lies just below the Fermi level at the H points, which is promising for tuning across the Fermi level in the near future.

We next measured the band structures of CoSn thin films in the $k_z = 0$ (mod 2π) plane by changing the photon energy to 128 eV. Different from the $k_z = \pi$ (mod 2π) plane in which two sets of flat bands can be observed, in the $k_z = 0$ (mod 2π) plane, only the FB2 can be seen, ∼0.3 eV below the Fermi level. The fitting results of the EDCs at multiple high-
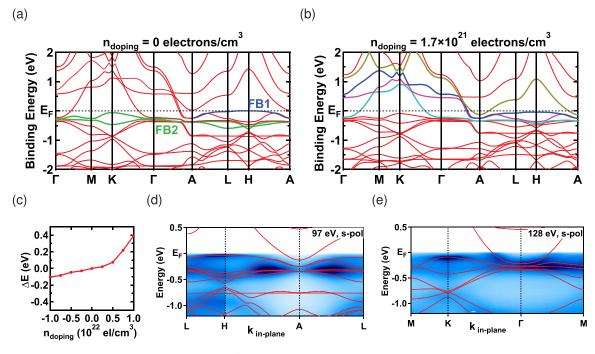
Figure 3. Density functional theory calculation results. (a) The band structure of pristine CoSn calculated by DFT. The horizontal dashed line represents the Fermi level. FB1 and FB2 are highlighted in blue and green, respectively. (b) The band structure of CoSn with doping of 1.7×10^{21} electrons/cm^3 and binding energy renormalization factor of 0.85. Bands I (cyan), II (pink), III (blue), and IV (gold) are the bands crossing the Fermi level. (c) Energy shift of FB1 at the H point as a function of the doping level. (d-e) DFT calculation results (red) overlaid on the ARPES spectra (blue image) taken at (d) $k_z = \pi$ and (e) $k_z = 0$, respectively. The DFT calculations show good agreement with the experimental data.
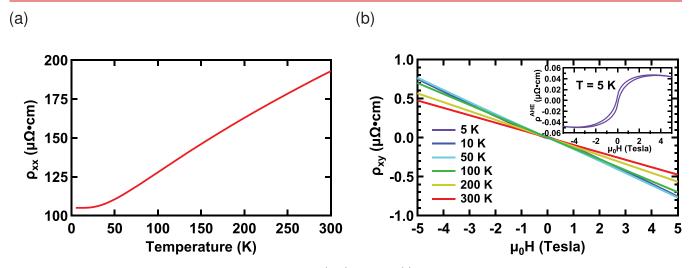

Figure 4. Transport properties of a 35 nm CoSn thin film on a MgO(111) substrate. (a) Longitudinal resistivity of the CoSn thin film as a function of temperature. (b) Hall resistivity of the CoSn thin film at different temperatures.

symmetry points across the first BZ suggest that the variation of FB2 binding energy is within ±0.03 eV, signifying the dispersionless nature of FB2 (see SI section S4.4).

An important question yet to be answered is whether the flat bands are topologically nontrivial for the CoSn thin films. Theoretically, the spin−orbit coupling (SOC) opens a gap between the flat band and quadratic band (QB) at the band touching point, making the flat band topologically nontrivial.[19−21] To verify this, we analyzed the spectrum around the Γ point, where FB2 touches the QB. The spectrum along the M-Γ-M direction ("Cut 1" in Figure 2c) in the first BZ clearly captures FB2 and the top QB, as shown in Figure 2d. Lorentzian fitting of representative EDCs along this direction

yields an SOC gap of 0.12 eV between FB2 and the top QB (Figure 2e). Meanwhile, the spectrum intensity of the bottom QB is maximized in the second BZ along the M′-Γ′-M′ direction ("Cut 2" in Figure 2c), as shown in Figure 2f. A similar analysis yields a 0.09 eV SOC gap between FB2 and the bottom QB (Figure 2g). Compared to the 0.04 to 0.08 eV SOC gap reported in CoSn bulk crystals,[5,6] the SOC gap for the thin film is slightly larger.

To investigate the tunability of the flat bands by carrier doping, we performed density functional theory (DFT) calculations (see SI Section S1.4 for methods). Figure 3a shows the band structure of pristine CoSn without carrier doping. This calculation suggests that FB1 sits exactly at the

Fermi level at the H point, while FB2 has a binding energy of −0.26 eV at the Γ point. We performed additional DFT calculations with different doping concentrations ranging from 1.0×10^{22} holes/cm^3 to 1.0×10^{22} electrons/cm^3 (see SI section S5). Within this doping range, adding electrons to the system ($n_{doping} > 0$) shifts the FB1 downward with respect to the Fermi level, while the band dispersion only changes slightly. The energy shift of FB1 at the H point as a function of the doping level is summarized in Figure 3c. We calculated the band structure with an arbitrary doping level by linearly interpolating the DFT results. Matching the binding energies of FB1 at the H point and FB2 at the Γ point yields a doping level of 1.7×10^{21} electrons/cm^3 and a binding energy renormalization factor of 0.85 (see Figure 3b). An overlay of DFT bands on top of the ARPES spectra shows good agreement between them, as shown in Figure 3d and 3e.

Figure 4a shows the longitudinal resistivity of a 35 nm CoSn thin film grown on a MgO(111) substrate as a function of temperature (see SI section 1.5 for methods). At room temperature, the CoSn thin film has a resistivity of 192 $\mu\Omega \cdot$ cm. As the temperature decreases from room temperature, the resistivity drops almost linearly down to ∼30 K and then reaches a plateau of 105 $\mu\Omega \cdot$cm. The Hall resistivity of the same sample at different temperatures is shown in Figure 4b. At room temperature, the Hall resistivity shows linear behavior with respect to the magnetic field with no detectable anomalous Hall effect. This observation is in agreement with the nonmagnetic nature of CoSn.[22] However, as the temperature drops below 10 K, an anomalous Hall effect starts to appear, although the amplitude is no larger than 0.05 $\mu\Omega \cdot$cm (see the inset of Figure 4b). This tiny anomalous Hall effect was also observed in sputtered thin films,[15] and similar signals were observed in low-temperature magnetization measurements of bulk crystals.[6] The mechanism behind it is suggested to be either a small deviation in stoichiometry or magnetism induced by the flat band.[15] The extracted carrier density is 6.57×10^{21} electrons/cm^3 at room temperature and 3.91×10^{21} electrons/cm^3 at 5 K, respectively.

The relationship between the transport properties and the band structure of CoSn has been discussed qualitatively;[5,6,14] however, a quantitative discussion has been missing. Meanwhile, it is important to quantitatively understand the relationship between the transport properties and the band structure of CoSn, especially to disentangle the contribution from individual bands, since the transport measurements provide indirect evidence for flat bands near the Fermi level.[14,17] Here, we provide an estimate of the Hall resistivity from DFT-calculated band structures. In semiclassical transport theory, the contribution to longitudinal conductivity σ_{xx} from band i is given by[23]

$$\sigma_{xx}^{(i)} = -\frac{e^2}{4\pi^3\hbar^2} \int \tau_i(\mathbf{k}) \left(\frac{\partial\varepsilon}{\partial k_x}\right)^2 \frac{\partial f}{\partial\varepsilon} d\mathbf{k} \tag{1}$$

where τ_i is the carrier relaxation time, $\varepsilon(\mathbf{k})$ is the energy dispersion, and f is the distribution function. Meanwhile, the contribution to Hall conductivity σ_H from band i is given by[23]

$$\sigma_H^{(i)} = -\frac{e^3}{4\pi^3\hbar^4} \int \tau_i(\mathbf{k}) \left(\frac{\partial\varepsilon}{\partial k_x}\right) \nabla_{\mathbf{k}}\varepsilon \times \nabla_{\mathbf{k}}\tau(\mathbf{k}) \left(\frac{\partial\varepsilon}{\partial k_y}\right) \frac{\partial f}{\partial\varepsilon} d\mathbf{k} \tag{2}$$

Since only partially occupied bands contribute to the transport at low temperatures, we hereby calculated the $\sigma_{xx}^{(i)}/\tau_i$ and $\sigma_H^{(i)}/\tau_i^2$ for the bands crossing the Fermi level, namely, bands I (cyan), II (pink), III (blue), and IV (gold) in Figure 3b (see SI section S6 for details). Assuming a universal and k-independent relaxation time τ for all bands, we calculated the Hall coefficient R_H by[23]

$$R_H = \frac{\sigma_H}{\sigma_{xx}^2} = \frac{\sum_i \sigma_H^{(i)}}{\left(\sum_i \sigma_{xx}^{(i)}\right)^2} \tag{3}$$

which is independent of relaxation time τ. With this method, our theory gives a Hall resistivity of -1.0×10^{-9} m^3/C, which has the same order of magnitude as the experimental value of -1.6×10^{-9} m^3/C at T = 5 K. The major contribution to the Hall coefficient comes from band I (see Table S2 in the Supporting Information), which has a large electron pocket around the Γ point. This analysis also yields values for σ_{xx} that are consistent with our experimental results if we assume reasonable values for τ, as discussed in SI section S6. Our theoretical modeling bridges the gap between the band structure and the experimentally measured transport properties of CoSn.

In conclusion, we synthesized epitaxial CoSn thin films directly on insulating substrates and studied their electronic band structures. The three-step growth generated highly ordered CoSn (0001) thin films, as confirmed by a combination of RHEED, XRD, and STEM. The electronic band structures of CoSn thin films were measured with synchrotron-based ARPES. The flat bands were clearly visualized, and the topologically nontrivial nature of the flat band is signified by the spin−orbit coupling gap at the band touching point. The ARPES measurement, DFT calculations, and transport properties of CoSn are consistent with each other not only qualitatively but also quantitatively. One very interesting direction in the near future will be the fabrication of devices that allow voltage gating in order to tune the flat bands across the Fermi level. This work makes the epitaxial CoSn thin films ready for studies of strongly correlated electronic states and flat band-induced phenomena.

■ METHODS

See SI section S1.

■ ASSOCIATED CONTENT

ⓢ Supporting Information

The Supporting Information is available free of charge at https://pubs.acs.org/doi/10.1021/acs.nanolett.3c01961.

> Methods (MBE, STEM, ARPES, DFT, transport measurements), RHEED and XRD of CoSn on MgO(111), additional STEM data, additional ARPES data, additional DFT calculations, and estimation of longitudinal conductivity and Hall conductivity (PDF)

■ AUTHOR INFORMATION

Corresponding Authors

David W. McComb − *Department of Materials Science and Engineering, The Ohio State University, Columbus, Ohio 43210, United States*; Email: mccomb.29@osu.edu

Igor Žutić − *Department of Physics, University at Buffalo, Buffalo, New York 14260, United States*; Email: zigor@buffalo.edu

Roland K. Kawakami − *Department of Physics, The Ohio State University, Columbus, Ohio 43210, United States;* orcid.org/0000-0003-0245-9192; Email: kawakami.15@osu.edu

Authors

Shuyu Cheng − *Department of Physics, The Ohio State University, Columbus, Ohio 43210, United States;* orcid.org/0000-0002-4784-4142

M. Nrisimhamurty − *Department of Physics, The Ohio State University, Columbus, Ohio 43210, United States*

Tong Zhou − *Department of Physics, University at Buffalo, Buffalo, New York 14260, United States*

Núria Bagués − *Department of Materials Science and Engineering, The Ohio State University, Columbus, Ohio 43210, United States*

Wenyi Zhou − *Department of Physics, The Ohio State University, Columbus, Ohio 43210, United States*

Alexander J. Bishop − *Department of Physics, The Ohio State University, Columbus, Ohio 43210, United States*

Igor Lyalin − *Department of Physics, The Ohio State University, Columbus, Ohio 43210, United States;* orcid.org/0000-0001-8076-8914

Chris Jozwiak − *Advanced Light Source, Lawrence Berkeley National Laboratory, Berkeley, California 94720, United States;* orcid.org/0000-0002-0980-3753

Aaron Bostwick − *Advanced Light Source, Lawrence Berkeley National Laboratory, Berkeley, California 94720, United States*

Eli Rotenberg − *Advanced Light Source, Lawrence Berkeley National Laboratory, Berkeley, California 94720, United States;* orcid.org/0000-0002-3979-8844

Complete contact information is available at:
https://pubs.acs.org/10.1021/acs.nanolett.3c01961

Author Contributions

S.C., M.N., W.Z., A.J.B., C.J., A.B., and E.R. performed ARPES measurements. S.C. and R.K.K. analyzed the ARPES data. S.C. performed MBE growth, transport measurements, and theoretical modeling of transport data. T.Z. and I.Ž performed DFT calculations. N.B. and D.W.M. performed STEM measurements. I.L. performed XRD measurements and fabricated devices. S.C. and R.K.K. conceived the project, and R.K.K. supervised the project. All authors contributed to writing the manuscript.

Notes

The authors declare no competing financial interest.

◼ REFERENCES

(1) Cao, Y.; Fatemi, V.; Fang, S.; Watanabe, K.; Taniguchi, T.; Kaxiras, E.; Jarillo-Herrero, P. Unconventional superconductivity in magic-angle graphene superlattices. *Nature* **2018**, *556*, 43−50.

(2) Yankowitz, M.; Chen, S.; Polshyn, H.; Zhang, Y.; Watanabe, K.; Taniguchi, T.; Graf, D.; Young, A. F.; Dean, C. R. Tuning superconductivity in twisted bilayer graphene. *Science* **2019**, *363*, 1059−1064.

(3) Wolf, T. M.; Lado, J. L.; Blatter, G.; Zilberberg, O. Electrically tunable flat bands and magnetism in twisted bilayer graphene. *Phys. Rev. Lett.* **2019**, *123*, No. 096802.

(4) Lu, X.; Stepanov, P.; Yang, W.; Xie, M.; Aamir, M. A.; Das, I.; Urgell, C.; Watanabe, K.; Taniguchi, T.; Zhang, G.; Bachtold, A.; MacDonald, A. H.; Efetov, D. K. Superconductors, orbital magnets and correlated states in magic-angle bilayer graphene. *Nature* **2019**, *574*, 653−657.

(5) Kang, M.; Fang, S.; Ye, L.; Po, H. C.; Denlinger, J.; Jozwiak, C.; Bostwick, A.; Rotenberg, E.; Kaxiras, E.; Checkelsky, J. G.; Comin, R. Topological flat bands in frustrated kagome lattice CoSn. *Nat. Commun.* **2020**, *11*, 4004.

(6) Liu, Z.; Li, M.; Wang, Q.; Wang, G.; Wen, C.; Jiang, K.; Lu, X.; Yan, S.; Huang, Y.; Shen, D.; Yin, J.-X.; Wang, Z.; Yin, Z.; Lei, H.; Wang, S. Orbital-selective Dirac fermions and extremely flat bands in frustrated kagome-lattice metal CoSn. *Nat. Commun.* **2020**, *11*, 4002.

(7) Lin, Z.; et al. Flatbands and emergent ferromagnetic ordering in Fe_3Sn_2 kagome lattices. *Phys. Rev. Lett.* **2018**, *121*, No. 096401.

(8) Yin, J.-X.; et al. Negative flat band magnetism in a spin−orbit-coupled correlated kagome magnet. *Nat. Phys.* **2019**, *15*, 443−448.

(9) Li, M.; Wang, Q.; Wang, G.; Yuan, Z.; Song, W.; Lou, R.; Liu, Z.; Huang, Y.; Liu, Z.; Lei, H.; Yin, Z.; Wang, S. Dirac cone, flat band and saddle point in kagome magnet YMn_6Sn_6. *Nat. Commun.* **2021**, *12*, 3129.

(10) Ye, L.; Fang, S.; Kang, M. G.; Kaufmann, J.; Lee, Y.; Denlinger, J.; Jozwiak, C.; Bostwick, A.; Rotenberg, E.; Kaxiras, E.; Bell, D. C.; Janson, O.; Comin, R.; Checkelsky, J. G. A flat band-induced correlated kagome metal. 2021, *arXiv.2106.10824 [cond-mat.mtrl-sci]*. https://doi.org/10.48550/arXiv.2106.10824 (accessed 2023-07-19),.

(11) Li, Z.; Zhuang, J.; Wang, L.; Feng, H.; Gao, Q.; Xu, X.; Hao, W.; Wang, X.; Zhang, C.; Wu, K.; Dou, S. X.; Hu, Z.; Du, Y. Realization of flat band with possible nontrivial topology in electronic Kagome lattice. *Science. Advances* **2018**, *4*, eaau4511.

(12) Han, M.; Inoue, H.; Fang, S.; John, C.; Ye, L.; Chan, M. K.; Graf, D.; Suzuki, T.; Ghimire, M. P.; Cho, W. J.; et al. Evidence of two-dimensional flat band at the surface of antiferromagnetic kagome metal FeSn. *Nat. Commun.* **2021**, *12*, 5345.

(13) Meier, W. R.; Du, M.-H.; Okamoto, S.; Mohanta, N.; May, A. F.; McGuire, M. A.; Bridges, C. A.; Samolyuk, G. D.; Sales, B. C. Flat bands in the CoSn-type compounds. *Phys. Rev. B* **2020**, *102*, No. 075148.

(14) Huang, H.; Zheng, L.; Lin, Z.; Guo, X.; Wang, S.; Zhang, S.; Zhang, C.; Sun, Z.; Wang, Z.; Weng, H.; Li, L.; Wu, T.; Chen, X.; Zeng, C. Flat-Band-Induced Anomalous Anisotropic Charge Transport and Orbital Magnetism in Kagome Metal CoSn. *Phys. Rev. Lett.* **2022**, *128*, No. 096601.

(15) Thapaliya, T.; Yoo, T.; Hurtado Parra, S.; Arndt, N. D.; Need, R.; Kikkawa, J. M.; Kim, H.; Huang, S. High-quality epitaxial thin films of topological kagome metal CoSn by magnetron sputtering. *Appl. Phys. Lett.* **2021**, *119*, No. 201902.

(16) Hong, D.; Liu, C.; Wen, J.; Du, Q.; Fisher, B.; Jiang, J.; Pearson, J. E.; Bhattacharya, A. Synthesis of antiferromagnetic Weyl semimetal Mn_3Ge on insulating substrates by electron beam assisted molecular beam epitaxy. *APL Materials* **2022**, *10*, 101113.

(17) Sales, B.; Meier, W.; May, A.; Xing, J.; Yan, J.-Q.; Gao, S.; Liu, Y.; Stone, M.; Christianson, A.; Zhang, Q.; McGuire, M. A. Tuning the flat bands of the kagome metal CoSn with Fe, In, or Ni doping. *Physical Review Materials* **2021**, *5*, No. 044202.

(18) Sales, B. C.; Meier, W. R.; Parker, D. S.; Yin, L.; Yan, J.; May, A. F.; Calder, S.; Aczel, A. A.; Zhang, Q.; Li, H.; et al. Chemical Control

of Magnetism in the Kagome Metal $CoSn_{1-x} In_x$: Magnetic Order from Nonmagnetic Substitutions. *Chem. Mater.* **2022**, *34*, 7069−7077.

(19) Sun, K.; Gu, Z.; Katsura, H.; Sarma, S. D. Nearly flatbands with nontrivial topology. *Phys. Rev. Lett.* **2011**, *106*, 236803.

(20) Guo, H.-M.; Franz, M. Topological insulator on the kagome lattice. *Phys. Rev. B* **2009**, *80*, 113102.

(21) Bolens, A.; Nagaosa, N. Topological states on the breathing kagome lattice. *Phys. Rev. B* **2019**, *99*, 165141.

(22) Allred, J.; Jia, S.; Bremholm, M.; Chan, B.; Cava, R. Ordered CoSn-type ternary phases in $Co_3 Sn_{3-x} Ge_x$. *J. Alloys Compd.* **2012**, *539*, 137−143.

(23) Hurd, C. M. *Hall effect in metals and alloys*; The International Cryogenics Monograph Series (INCMS); Plenum Press: New York, 1972; p 72.